Durable 3–5 μm transmitting infrared window materials

Daniel C. Harris

Chemistry and Materials Branch, Research and Technology Division, Naval Air Warfare Center Weapons Division, China Lake CA 93555, USA

Abstract

Properties of 3–5 μm infrared-transmitting window materials are reviewed, with an emphasis on durable materials for applications in environments involving moisture, impact by solid and liquid particles, high temperatures and rapid heating rates. Infrared, visible and ultraviolet transmission windows are compared for MgF_2, aluminum oxynitride, sapphire, spinel, MgO, Y_2O_3, calcium aluminate, SiO_2, CaF_2, LiF, ZnS, ZnSe, GaAs, GaP, Si and Ge. Emission at elevated temperature, reflection and optical scatter are also discussed. A comparison of mechanical and thermal properties is given, as is a brief discussion of rain and particle erosion resistance. © 1998 Elsevier Science B.V. All rights reserved.

Keywords: Infrared; Ultraviolet; Visible; MgF_2

1. Introduction

Excellent optical quality single-crystal materials such as sodium chloride and potassium bromide have been available for many decades as infrared-transparent windows for laboratory use. However, poor mechanical properties and susceptibility to attack by water prohibit the use of these materials in all but the most benign environments. For this reason, there has been a continuing search for more robust materials that can be used in environments involving moisture, impact by solid and liquid particles, high temperatures and rapid heating rates. This review emphasizes durable materials available for the 3–5 μm (midwave) atmospheric infrared transmission window. Some '2-color' materials that have good transmission in both the midwave and 8–14 μm (long wave) atmospheric windows will also be discussed.

Table 1 lists many infrared window materials and indicates whether common forms are available as single crystals, polycrystalline materials, or glasses.

Most window materials are electrical insulators, but Ge, Si, GaAs and GaP have sufficiently small bandgaps (0.7, 1.1, 1.4 and 2.2 eV) that their optical properties are degraded at temperatures well below their chemical stability limits. Major sources of information on infrared window materials are listed in Refs. [1–8].

2. Transmission window

Figs. 1–5 compare the infrared transmission of window materials on wavenumber and wavelength scales. In Fig. 1, sapphire, ALON (aluminum oxynitride), spinel and yttria are representative of the best optical quality available for each material. Magnesium fluoride in Fig. 1 is hot pressed, polycrystalline Irtran-1®, a material formerly sold by Kodak. The spectrum of this material, which is representative of currently available hot pressed MgF_2, exhibits a sharp impurity band at 3565 cm^{-1} and a weak,

Table 1
Three classes of infrared window materials

Single crystal	Polycrystalline	Glass
LiF	MgF$_2$	Calcium aluminate (Ca–Al–Ba–O)
NaCl	ZnS	As$_2$S$_3$
KCl	CaF$_2$	Fused silica (SiO$_2$)
AgCl	ZnSe	Germanate glass (Ge–Al–Ca–Ba–Zn–O)
MgF$_2$	MgO	Fluoride glass (Zr–Hf–Ba–F)
CaF$_2$	CdTe	Chalcogenide glasses (Ge–Si–S–Se–Te)
BaF$_2$	MgAl$_2$O$_4$ (spinel)	AMTIR® (Ge–As–Se)
CsI	9Al$_2$O$_3$ · 5AlN (ALON)	
Si	Y$_2$O$_3$	
Ge	Lanthana-doped Y$_2$O$_3$	
Quartz	Si	
Sapphire	Ge	
GaAs	GaAs	
	GaP	

Hot pressed polycrystalline windows were formerly sold by Kodak under the following trade names: Irtran-1 (MgF$_2$), Irtran-2 (ZnS), Irtran-3 (CaF$_2$), Irtran-4 (ZnSe), Irtran-5 (MgO) and Irtran-6 (CdTe).

broad impurity band centered near 3500 cm^{-1}. Both bands probably arise from OH impurities. Magnesium oxide in Fig. 1 (Kodak Irtran-5) is a low quality hot-pressed material with a broad impurity band at 3000–3500 cm^{-1} and sharper impurity bands at 1550 and 1320 cm^{-1}. These bands are not seen in single-crystal MgO [9]. The most important comparison in Fig. 1 is the long wave cutoff, which increases in the order ALON < sapphire < spinel < MgO ≈ Y$_2$O$_3$ < MgF$_2$. The shorter the cutoff wavelength,

the less useful the window is at elevated temperature. The loss of transmittance with decreasing wavelength in the spectra of MgF$_2$ and Y$_2$O$_3$ is attributed to Rayleigh optical scattering by centers that are smaller than the wavelength of light.

Fig. 2 shows that calcium aluminate glass, quartz (crystalline SiO$_2$) and fused silica (SiO$_2$ glass) all have shorter wavelength cutoffs than sapphire. Calcium aluminate also has a strong band near 3000–3500 cm^{-1} that is probably due to OH groups. The
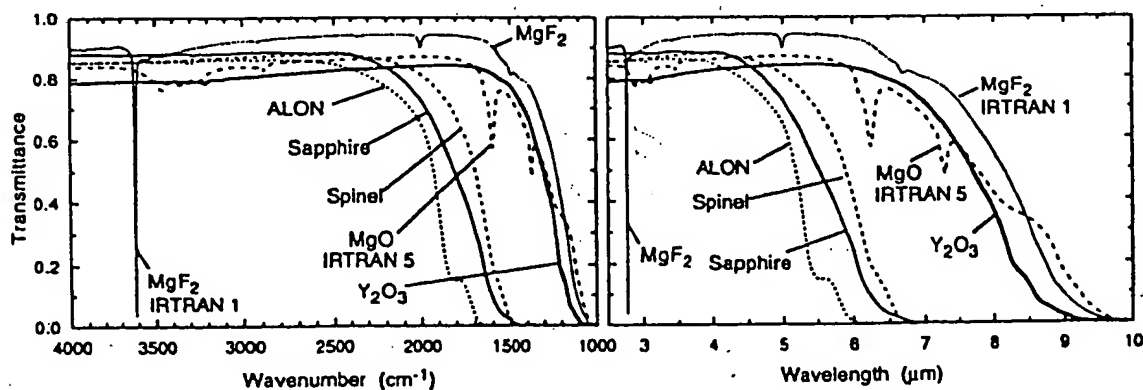

Fig. 1. Infrared transmittance of magnesium fluoride (Kodak hot pressed Irtran-1®, 2.0 mm thick), aluminum oxynitride (Raytheon polycrystalline ALON, 1.9 mm thick), sapphire (Union Carbide single crystal, 60° cut, 2.6 mm thick), spinel (Coors polycrystalline MgAl$_2$O$_4$, 1.7 mm thick), magnesium oxide (Kodak hot pressed Irtran-5®, 2.1 mm thick) and yttrium oxide (Raytheon polycrystalline yttria, 2.1 mm thick).
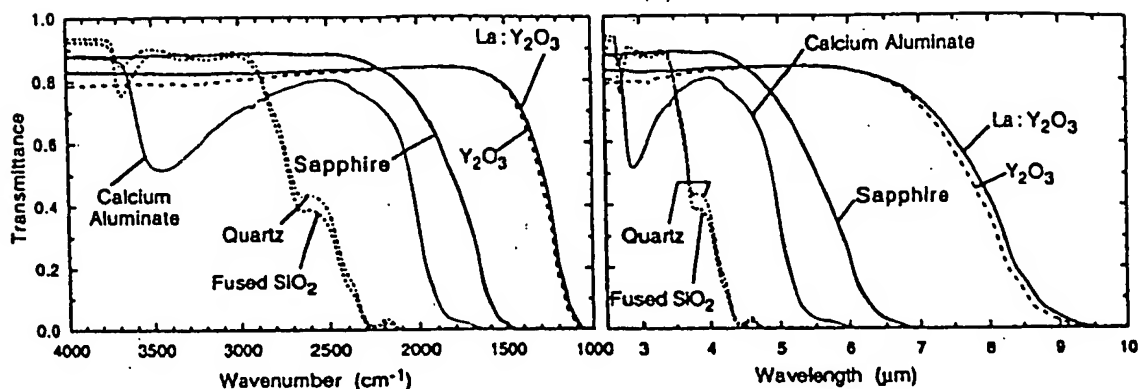
Fig. 2. Infrared transmittance of calcium aluminate glass (unknown source, 2.6 mm thick), quartz (single crystal, 4.7 mm thick), fused silica (unknown source, 5.3 mm thick), sapphire (Union Carbide single crystal, 60° cut, 2.6 mm thick), yttria (Raytheon polycrystalline Y_2O_3, 2.1 mm thick) and lanthana-doped yttria (GTE polycrystalline $0.09La_2O_3 \cdot 0.91Y_2O_3$, 1.9 mm thick).
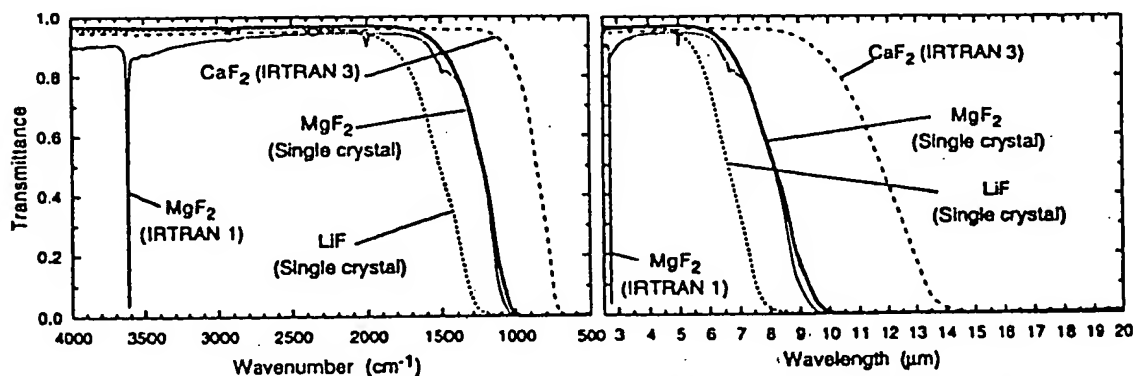

Fig. 3. Infrared transmittance of magnesium fluoride (Kodak hot pressed Irtran-1®, 2.0 mm thick), magnesium fluoride (John H. Ransom Laboratories single crystal, 2.7 mm thick), lithium fluoride (Harshaw single crystal, 5.4 mm thick) and calcium fluoride (Kodak hot pressed Irtran-3®, 1.1 mm thick).
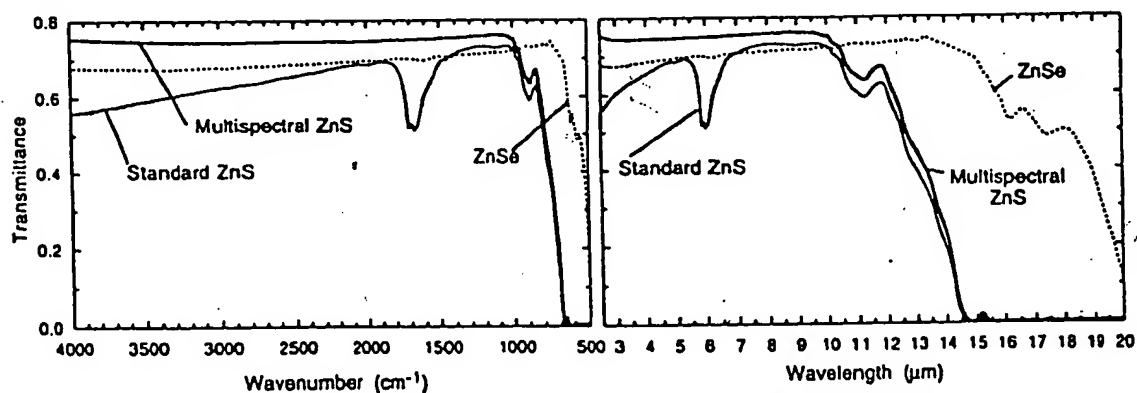

Fig. 4. Infrared transmittance of standard grade zinc sulfide (Raytheon polycrystalline material, 6.0 mm thick), multispectral grade zinc sulfide (Raytheon polycrystalline material, 5.2 mm thick) and zinc selenide (Raytheon polycrystalline material, 7.1 mm thick).
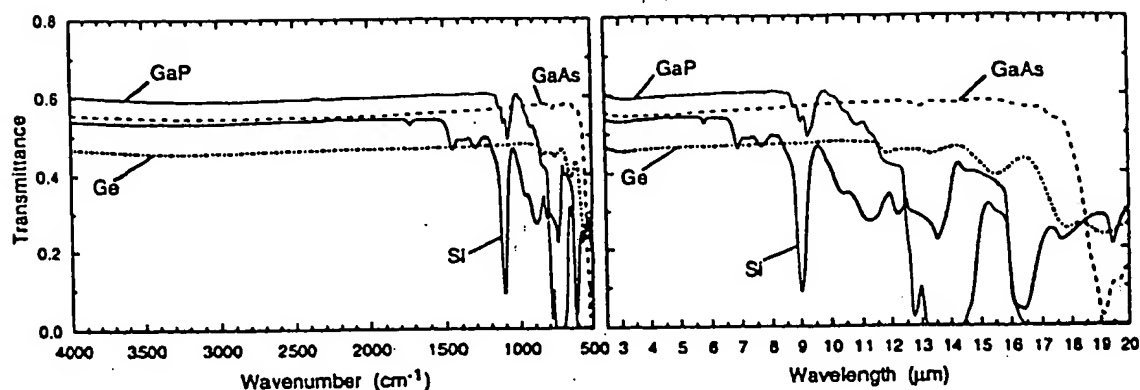
Fig. 5. Infrared transmittance of germanium (2.8 mm thick), silicon (2.8 mm thick), gallium phosphide (Texas Instruments polycrystalline material, 3.0 mm thick) and gallium arsenide ((100) single crystal, 0.65 mm thick).

infrared spectrum of lanthana-doped yttria (poly-crystalline material with the composition $0.09La_2O_3 \cdot 0.91Y_2O_3$) is nearly identical to that of yttria.

Fig. 3 shows that single-crystal MgF_2 has the same long-wave cutoff as polycrystalline MgF_2, but lacks the impurity bands seen in Irtran-1. The cutoff for LiF is at shorter wavelength and that of CaF_2 is at longer wavelength, relative to MgF_2. These materials illustrate the general trend that the long-wave cutoff tends toward longer wavelength as the atoms in a structure become heavier (Li < Mg < Ca).

Fig. 4 compares ZnSe with two varieties of ZnS. These materials are available today as chemical-vapor-deposited, polycrystalline materials. (The historically important hot pressed ZnS, Irtran-2, is no longer available.) ZnSe, an excellent '2-color' (3–5 and 8–14 μm) window material with extremely low absorption, is not as durable as ZnS. Standard grade (yellow) ZnS is useful in part of the 8–14 μm region, but significant optical scatter reduces its utility in the 3–5 μm region. However, Multispectral® (colorless) ZnS (also called Cleartran® and Waterclear® ZnS), prepared by heat treatment of standard ZnS, has low optical scatter in the 3–5 μm window. Standard ZnS has a band near $1700 \ cm^{-1}$ attributed to stretching of Zn–H impurities [10].

The semiconductor materials Ge and GaAs in Fig. 5 are excellent optical windows for both the 3–5 and 8–14 μm regions at 20°C. However, free carrier absorption becomes significant in Ge above 100°C [11] and in GaAs above 400°C [12]. GaP is an excellent 3–5 μm window up to 600°C, but has

significant intrinsic absorptions in the 8–14 μm region [13]. Si is also a good 3–5 μm window up to about 250°C [11], but has numerous absorptions in the 8–14 μm region. Many of these absorptions are attributed to oxygen impurities. It is reported that float-zone growth of single crystal Si, a technique that eliminates quartz crucibles as a source of oxygen, produces Si that is free of impurity bands in the 8–14 μm range [14].

The ultraviolet and visible optical windows of the materials in Figs. 1–5 are shown in Figs. 6–8. Sapphire in Fig. 6 has excellent ultraviolet optical quality. Lower grades of sapphire have an absorption
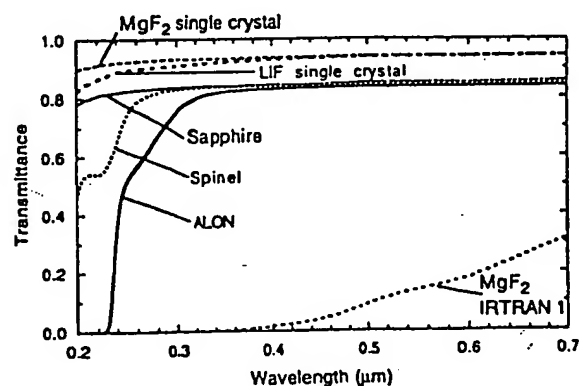

Fig. 6. Ultraviolet/visible transmittance of single-crystal MgF_2, (John H. Ransom Laboratories, 2.7 mm thick), polycrystalline MgF_2 (Kodak hot pressed Irtran-1®, 2.0 mm thick), single-crystal LiF (5.4 mm thick), sapphire (Union Carbide single crystal, 60° cut, 2.6 mm thick), spinel (Coors polycrystalline $MgAl_2O_4$, 1.7 mm thick) and polycrystalline ALON (Raytheon, 1.9 mm thick).
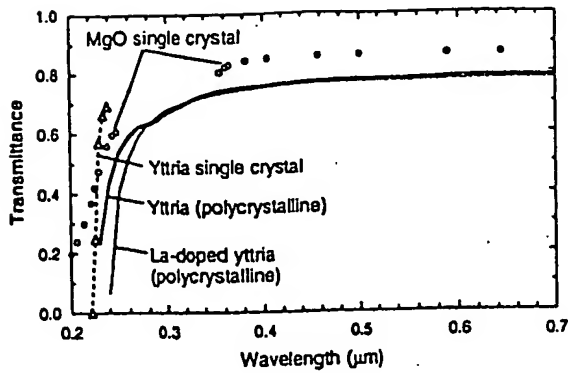
Fig. 7. Ultraviolet/visible transmittance of polycrystalline yttria (Raytheon Y_2O_3, 2.0 mm thick), polycrystalline lanthana-doped yttria (GTE $0.09La_2O_3 \cdot 0.91Y_2O_3$, 2.0 mm thick), single crystal MgO and single crystal Y_2O_3. Spectra of 2.0 mm thick single crystal materials were computed from the optical constants n and k given by Palik [8] using Eqs. (1)–(3).

band centered at 205 nm [15]. Fig. 7 compares the performance of an excellent optical quality specimen of polycrystalline yttria to tabulated data for single-crystal yttria. It is typical of polycrystalline materials to cut off in the ultraviolet region at longer wavelength than a single crystal. This is likely due to optical scatter. Fig. 8 shows that silica, quartz, CaF_2, calcium aluminate and multispectral zinc sulfide transmit throughout the visible region. ZnSe and GaP
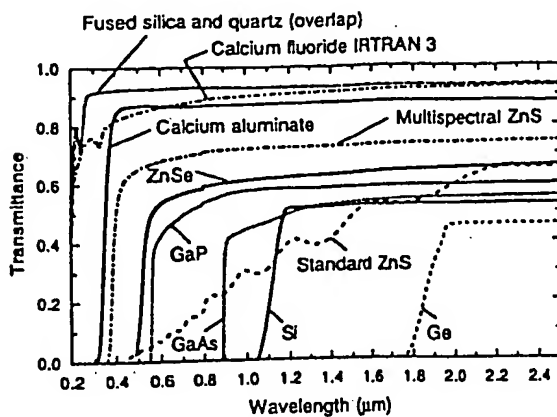
provide just part of the visible window, while GaAs, Si and Ge cut off in the near infrared.

Tabulated [7,8] optical constants used to reconstruct the transmittance of single crystal MgO and Y_2O_3 in Fig. 7 are n and k, the real and imaginary parts of the refractive index. To convert n and k to transmittance, the following formulas were used:

Single surface normal reflectance (R):

$$R = \frac{(1-n)^2 + k^2}{(1+n)^2 + k^2}.$$ (1)

Absorption coefficient (α):

$$\alpha = 4\pi k/\lambda \quad (\lambda = \text{wavelength}).$$ (2)

Transmittance (T):

$$T = \frac{(1-R)^2 e^{-\alpha b}}{1 - R^2 e^{-2\alpha b}} \quad (b = \text{sample thickness}).$$ (3)

Eq. (3) presumes that scatter is negligible, which may not be true at ultraviolet wavelengths. The absorption coefficient (α) and sample thickness (b) are customarily expressed in units of cm^{-1} and cm, respectively. Other parameters in Eqs. (1)–(3), except wavelength, are dimensionless.

In high quality windows, bulk absorption is low enough that a significant fraction of absorption oc-

Fig. 8. Ultraviolet/visible/near infrared transmittance of quartz (4.7 mm thick), fused silica (5.3 mm thick), CaF_2 (Kodak Irtran-3®, 1.1 mm thick), calcium aluminate glass, (2.6 mm thick) multispectral ZnS (Raytheon, 5.2 mm thick), ZnSe (Raytheon, 7.1 mm thick), GaP (Texas Instruments, 3.0 mm thick), standard ZnS (Raytheon, 6.0 mm thick), GaAs (single crystal, 0.65 mm thick), Si (2.8 mm thick) and Ge (2.8 mm thick).
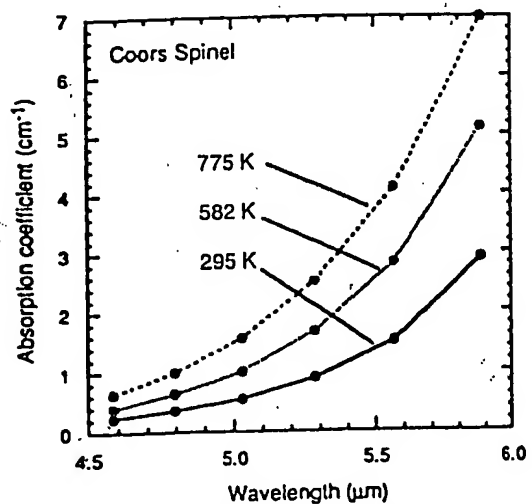

Fig. 9. Temperature dependence of long wave absorption edge of Coors spinel [22]. In general, the absorption edge for most materials shifts to shorter wavelength as temperature increases.

curs at the surfaces. For example [16,17], at a wavelength of 5.25 μm, 1-cm thick polycrystalline, cast CaF$_2$ absorbs 0.042% of the light in the bulk and absorbs 0.0028% at the two surfaces. In the case of polycrystalline 'FLIR-grade' ZnSe at 8 μm wavelength, a 1-cm thick window absorbs 0.06% of the light in the bulk and 0.3% of the light at the two surfaces [18].

3. Emission at elevated temperature

For use at high temperature, the most important limitation of an infrared window is emission of light

from the window itself. Emission can exceed the signal being observed, especially since the window is much closer to the detector than the object being viewed. Emission has been reported for Irtran-1, Irtran-2 and Irtran-3 hot pressed materials [19], and for sapphire, yttria, spinel, ALON and fused silica [20,21]. Emission is related to absorption: the greater the absorption at a given wavelength, the greater the emission.

In general, the long wave absorption edge of an infrared window material shifts to shorter wavelength as the temperature rises. Fig. 9 illustrates this point for spinel [22]. For use in the 3–5 μm atmo-
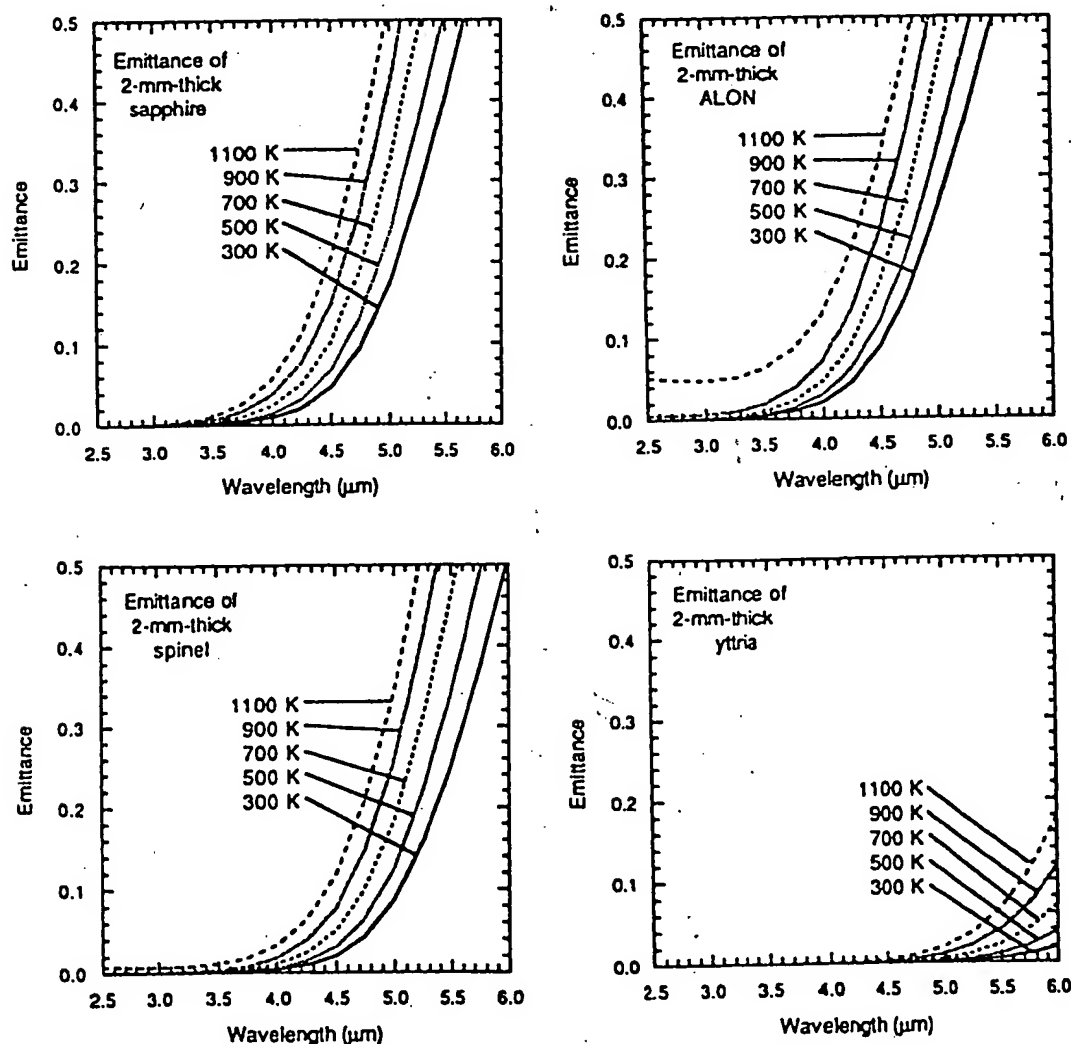

Fig. 10. Emittance of window materials computed with Eq. (4) using absorption coefficients computed by the program *Optimatr* [26].
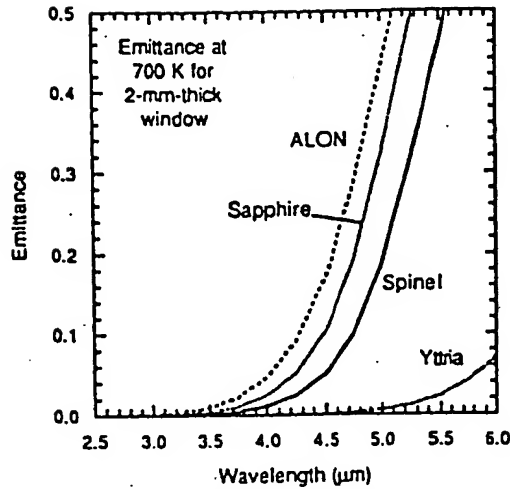
Fig. 11. Comparison of calculated emittance of ALON, sapphire, spinel and yttria at 700 K using absorption coefficients computed with *Optimatr* [26]. Note the correspondence between emittance and the long wave cutoff behavior in Fig. 1.

spheric window, an important comparison in Fig. 1 is the long wave cutoff, which increases in the order ALON < sapphire < spinel < MgO ≈ Y_2O_3 < MgF_2. At room temperature, each of these windows can be used at wavelengths close to the cutoff. At elevated temperature, there is significant emission near the cutoff and the cutoff shifts to shorter wavelength.

For a window with absorption coefficient α, thickness b, and single-surface normal reflectance R (Eq. (1)), the normal emittance is given by

Emittance (ε):

$$\varepsilon = \frac{(1-R)(1-e^{-\alpha b})}{1 - Re^{-\alpha b}} \approx \alpha b \quad (\text{for } \alpha b \leq 0.1)$$

$$(4)$$

A blackbody has an emittance of 1, whereas a perfectly transparent window has an emittance of 0. If we know the absorption coefficient of a material as a function of temperature, we can use Eq. (4) to compute the emittance as a function of temperature.

A multiphonon model for the absorption of window materials near the long wave cutoff has been developed [23,24] and implemented in a computer code [25] sold under the name *Optimatr*® [26].

Absorption coefficients computed by this code closely match those measured for oxide and halide window materials over a wide range of temperature. From calculated absorption coefficients, Eq. (4) was used to compute the emittance of sapphire, ALON, spinel and yttria in Fig. 10. Just as the absorption edge shifts to shorter wavelength with increasing temperature in Fig. 9, the emission edge also shifts to shorter wavelength with increasing temperature in Fig. 10. Fig. 11 compares the emission edges of the four materials of Fig. 11 at a single temperature. The important point is that the shorter the wavelength of the cutoff in the absorption spectrum, the shorter the wavelength of the emission edge.

There is an important limitation on the use of the multiphonon model for absorption and emission. The model is based on the behavior of the absorption edge where the intrinsic absorption of the material dominates over effects of impurities and crystal defects. In the window region where the material of interest has no significant absorption, impurities and defects dominate the observed optical behavior. For example, Fig. 12 compares the measured [27] emittance of yttria at 1000°C with that calculated by *Optimatr*. The calculated emittance is negligible at wavelengths shorter than 4.5 μm. The observed
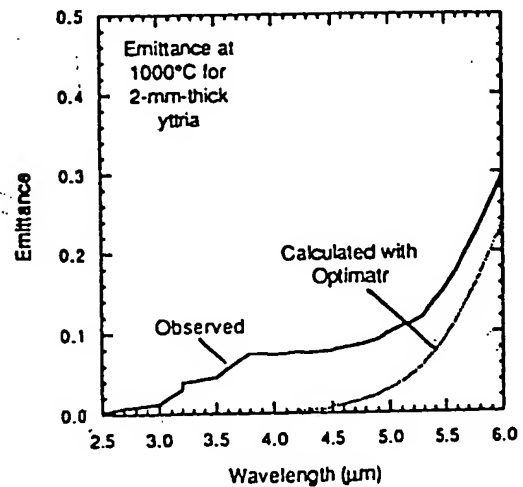

Fig. 12. Comparison of measured [27] emittance of yttria at 1000°C with that calculated by *Optimatr* [26] using Eq. (4).

Table 2
Refractive index and absorption coefficient near 300 K

Material	Wavelength			dn/dT^a $(10^{-6}\,K^{-1})$	Flat plate transmittance[b]	Absorption coefficient[d] at 4 μm (cm^{-1})
	0.5 μm	4 μm	10 μm			
ALON (polycrystalline) [8]	1.80	1.702	–	3	0.874	0.10 [26]
AMTIR-1 (Ge$_{33}$As$_{12}$Se$_{55}$) [2]	–	2.515	2.498	80	0.687	0.002 [30]
Calcium aluminate glass (Barr and Stroud 37A) [31]	1.678	1.607	–	–	0.897	0.19 [31]
Calcium fluoride [8]	1.436	1.410	1.306	–10 [32,33]	0.944	<0.001 [26]
Fused silica [7]	1.462	1.389	–	10 [34]	0.948	–
Gallium arsenide [7]	4.305	3.304	3.274	150	0.554	<0.01 [35]
Gallium phosphide [7]	3.590	3.014	2.964	137[a]	0.598	<0.01 [12]
Germanate glass [36] (Corning 9754, Ge–Al–Ca–Ba–Zn–oxide)	1.68	1.605	–	–	0.898	–
Germanium [7]	4.388	4.025	4.004	400 [37]	0.468	<0.01 [38]
Lithium fluoride [7]	1.394	1.349	–	–15 [28]	0.957	<0.006 [7]
MgF$_2$ (single crystal) [8]	1.380 (n_o), 1.392 (n_e)	1.349 (n_o), 1.359 (n_e)	–	1, 0.6 [28]	0.957	0.001 [26]
MgO (single crystal) [8]	1.745	1.668	–	19 [39]	0.882	0.001 [8]
Sapphire [26]	1.774 (n_o), 1.766 (n_e)	1.677 (n_o), 1.667 (n_e)	–	6 [88], 12 [40]	0.880	0.047 [26]
Silicon [7]	4.298	3.429	3.422	170 [28,41]	0.538	<0.005 [7]
Silicon carbide (cubic) [8]	2.664	2.492 [26]	–	–	–	–
Silicon carbide (6H) [7]	2.686 (n_o), 2.732 (n_e)	2.516 (n_o)	–	–	0.686	20 [7]
Spinel (polycrystalline) [8]	1.723	1.635	–	3	0.890	0.018 [26]
Yttria (single crystal Y$_2$O$_3$) [8]	1.947	1.859	–	8 [8], 31[c]	0.834	0.04 [42][d]
Yttria (La-doped) [42] (Polycrystalline 0.09La$_2$O$_3$·0.91Y$_2$O$_3$)	1.937	1.847	–	32 [43]	0.837	0.04 [42][d]
Zinc sulfide (CVD) [44,7]	2.420	2.252	2.200	40	0.742	0.02 [45]
Zinc sulfide (multispectral)	–	–	–	–	–	~0.001 [46]
Zinc selenide (CVD) [8,44]	2.7	2.433	2.406	60	0.703	0.0016 [45]

[a] Temperature dependence (dn/dT) applies at infrared wavelengths, generally in the 3–5 μm region.
[b] At 4 μm wavelength calculated with Fig. 5.
[c] Measured on polycrystalline yttria and lanthana-doped yttria at GTE Laboratories [47].
[d] At 3.39 μm wavelength.
[e] Raytheon/Texas Instruments data, 1998.

Table 3
Optical scatter

Material	Thickness (mm)	Total integrated scatter (%) (forward hemisphere)			Total integrated scatter (%) (backward hemisphere)		
		0.64 μm[a]	1.15 μm	3.39 μm	0.64 μm[a]	1.15 μm	3.39 μm
ALON (polycrystalline, Raytheon) [49]	5.1	2.1	2.9	1.0	—	—	—
ALON (polycrystalline, Raytheon) [49]	2.0	0.2	—	0.05	—	—	—
ALON (polycrystalline, Raytheon) [50]	5.1	3.1	—	2.2	—	—	0.2
ALON (polycrystalline, Raytheon) [51]	1.0	4.5	3.9	1.1	0.6	1.6	—
GaP (AR coated, Texas Instruments)[b]	5.1	0.6	—	1.2	—	—	0.04
Germanate glass (Corning 9754) [50]	5.1	0.6	—	0.2	—	—	—
MgF$_2$ (polycrystalline, domes) [48]	3.0	—	—	1.3	—	—	—
MgF$_2$ (polycrystalline)[b]	2.5	23	—	2	4	—	0.4
MgF$_2$ (single crystal) [50]	3.4	0.0015	—	—	—	—	—
Sapphire (Crystal Systems) [49]	5.1	0.025	0.017	—	—	—	—
Sapphire [51]	3.2	0.26	0.017	—	0.12	—	—
Spinel (polycrystalline, Coors) [49]	5.1	7.2	3.4	0.1	—	—	—
Spinel (polycrystalline, Coors)[b]	1.7	0.5	—	0.4	—	—	—
Spinel (polycrystalline, Coors) [50]	5.1	3.4	—	0.8	—	—	0.05
Spinel (polycrystalline, Raytheon) [49]	5.1	2.6	1.4	—	—	—	—
TAF-1 fluoride glass (Hoya) [49]	5.1	0.15	0.10	0.4	—	—	—
Yttria (polycrystalline, Raytheon) [42]	2.0	3	2	1.3	—	—	—
Yttria (La-doped, polycrystalline, GTE) [42,52]	2.0	4	—	—	—	—	—
Yttria (La-doped, polycrystalline, GTE) [49]	5.1	4.3	2.8	0.9	—	—	—
ZnS (multispectral, polycrystalline, Raytheon)[b]	5.2	—	—	0.3	—	—	0.07
ZnS (standard grade, polycrystalline, Raytheon)[b]	6.0	—	—	8.3	—	—	2.0

[a] Measurement at either 0.633 or 0.647 nm.
[b] Unpublished China Lake measurement.

Table 4
Physical properties

Material	Strength (MPa)	Knoop hardness (kg/mm²)	Modulus (GPa)	Poisson's ratio	Thermal conductivity (W/m K)	Expansion coefficient $(10^{-6}\,K^{-1})$	Density (g/ml)	Melting point (K)	Heat capacity (J/g K)
ALON (polycrystalline, Raytheon) [54]	300 (20°C), 270 (1000°C)	1950 (200 g load)	323	0.24	12.6 (25°C) [55], 7.1 (270–830°C)	7.5 (30–900°C)	3.68	2425	0.77
AMTIR-1 ($Ge_{33}As_{12}Se_{55}$) [30,3]	19	170	22	0.27	0.25	12	4.4	573 [a]	0.29
Calcium aluminate glass [31] (Barr and Stroud BS37A)	90	726	109	0.29	1.2	8.3 (20–200°C)	2.90	993 [a]	0.85
CaF_2 (single crystal) [56]	37	~170	76		9.7 (36°C)	19 [57]	3.18	1668	0.85 (0°C)
Fused silica (Corning 7940) [58] or Dynasil [59]	50 (25°C) [59], 75 (900°C) [59]	600 [59]	72 [58]	0.16 [58]	1.4 [59]	0.51 (0–300°C) [58]	2.20		0.74
Gallium arsenide [35,60]	130	750	86–144	0.33	53 (25°C), 33 (200°C)	5.7 (25°C), 6.4 (200°C)	5.32	1511	0.33
GaP [61,12]	100	834	143, 103	0.31	97	5.3, 6.2	4.13	1740	0.84 (127°C)
Germanate glass (Corning 9754) [62]	90–100	512	103	0.28		5.9	3.58		0.56
Germanium [63,4]		780	65	(0.27)	60	37 (0–100°C)	5.32	1210	0.31
Lithium fluoride [56]		110	115		11.3 (41°C)	11 (25–200°C)	2.64	1121	1.56
MgF_2 (polycrystalline Irtran-1) [64]	150, 80 [c] [65], 130 [c] [65]	575			15 (56°C)	13.7 (∥c), 8.5 (⊥c)	3.18	1528	0.96
MgF_2 (single crystal) [56]	50	415	138	0.27	30		3.18	1528	1.00

Material									
Magnesium oxide [4]	700 [68,69]	690	249	0.18	59	11	3.58	3070	0.88
Sapphire [66,67]	~200 (800°C) [68,69]	1500–2200	345–386	0.29	42 (25°C) [70] 18.9 (327°C) [70] 11.5 (627°C) [70]	6.66 (‖c) 5.0 (⊥ c)	3.98	2300	0.78 (27°C) [71] 1.17 (497°C) [71]
Silicon [72,73,4]	70–340 [73]	1150	131	0.28	148	2.6 [57]	2.33	1685	0.76
Silicon carbide (CVD)[b] [74]	600	2500	466	0.21	144	1.9	3.21	–	0.70
Spinel (polycrystalline) [75]	100–200	1400	273	0.26	14.8 (100°C) 5.4 (1200°C)	5.6 (25–200°C) 7.9 (25–1000°C)	3.58	2400	0.88
Yttria (polycrystalline) [42,76]	150 ~150 (1400°C)	720	174	0.30	13.5 (27°C) 6.4 (327°C)	6.5 (27°C) 7.0 (327°C)	5.03	2710	0.48 (27°C) 0.52 (327°C)
Yttria (La-doped) [42,76]	165 ~165 (1400°C)	760	168	0.30	5.3 (27°C) 3.9 (327°C)	6.5 (27°C) 7.0 (327°C)	5.13	2670	0.48 (27°C) 0.52 (327°C)
ZnS (multispectral) [46,77]	69, 60	160	88, 74	0.32, 0.28	27	6.5 (–65–200°C) 7.5 (200°C)	4.08	2130	0.52
ZnS (standard grade) [46,78]	97, 95 204 (200°C) 220 (600°C)	230, 250	74	0.29, 0.27	17, 16 10 (200°C) 7 (600°C)	6.8 (25°C) [77] 7.7 (200°C) [77]	4.08	2130	0.47
ZnSe [46,77]	52, 55	105, 120	70, 67	0.28	18	7.3 (25°C) 8.3 (200°C)	5.27	1790	0.34

[a] Upper use temperature.
[b] Chemical vapor deposited.
[c] The value 130 MPa is the strength at 25°C of 4-point bend bars with width = thickness = 0.178 mm, load span = 25.4 mm and support span = 0.85 mm. The value 80 MPa applies to equibiaxial flexure disks with a load diameter of 38.1 mm, support diameter of 79.4 mm and disk diameter of 85.1 mm.

emittance has a plateau with $\varepsilon \approx 0.08$ stretching from 3.5 to 5 μm. Although OH impurities in Y_2O_3 could be expected to give rise to absorption and emission near 3 μm, it is not clear how to account for emission in the 4–5 μm region. The lesson from Fig. 12 is that the emittance of a window material in its window region must be measured and cannot be accurately modeled. If the measured and modeled behavior are in agreement over some range of temperature, it is probably safe to extrapolate the model to other temperatures to predict window performance.

The example in Fig. 12 was chosen to illustrate poor agreement between measured and calculated emittance. Spinel, ALON and ultraviolet-grade sapphire show excellent agreement between theoretical and measured emittance at wavelengths as short as 3 μm, with no obvious impurity emission [20,21]. By contrast, a lower grade of sapphire has an emission band centered near 3 μm that is not predicted by the model [20,21].

4. Refractive index

Good sources of information on refractive index of optical materials are available [26,28,29]. Table 2 lists the refractive index (n) of many midwave infrared materials near 20°C, and indicates the temperature dependence (dn/dT). Single crystals of sapphire, MgF_2 and hexagonal SiC have 3- or 6-fold axes of symmetry called the optical axis or the ordinary direction. The refractive index in the direction of the 3- or 6-fold axis is designated n_o. The refractive index on the 2-fold symmetry axis perpendicular to the optical axis is designated n_e. Other materials in Table 2 have isotropic refractive index.

In Table 2, fluorides have the lowest refractive index, followed closely by oxides. Materials with heavier atoms have higher refractive index. Oxides and fluorides have a relatively small temperature dependence dn/dT. The chalcogenides (ZnS, ZnSe, AMTIR) have greater values of dn/dT and the semiconductors (Ge, Si, GaAs, GaP) have the greatest temperature dependence.

The higher the refractive index, the greater the reflection loss. The theoretical transmittance in air of a flat plate with no absorption or scatter loss is given by

Transmittance of flat plate (t):

$$t = \frac{2n}{n^2 + 1}.\qquad(5)$$

Table 2 lists the transmittance calculated with Eq. (5). This reflection-limited transmittance accounts for the different values of baseline transmission observed in Figs. 1–5.

5. Optical scatter

Light striking an ideal optical window at normal incidence is transmitted through the window with no change in direction. In all real materials, some light is scattered in all directions from both surfaces and from the bulk of the optical window.

Total integrated scatter (TIS) [48] in Table 3 is measured with an integrating sphere by collecting all light scattered between 2.5° and 70° from the normal direction in either the forward hemisphere or the back hemisphere. Light scattered < 2.5° is considered to be specular for the sake of this measurement. Light scattered by more than 70° is generally negligible. TIS is a dimensionless ratio of the power (W) of scattered light divided by the power of incident light (measured with no sample in the beam). TIS can be measured in either the forward (transmitted) or backward (reflected) hemisphere.

An alternate measurement called bidirectional transmittance distribution function (BTDF) [53] measures scattered light as a function of angle. BTDF is defined as $(P_s/P_i)/(\Omega \cos \theta)$, where P_s is the power of scattered light, P_i is the power of incident light, θ is the scattering angle measured from the incident (normal) direction, and Ω is the solid angle of scatter viewed by the detector. When θ is very small, the detector collects specularly transmitted light. As θ increases from zero, the detector collects scattered light whose intensity decreases rapidly with angle. By integrating the scattered light from 2.5° to 70°, the BTDF measurement gives results similar to the TIS measurement, as verified with lanthana-doped yttria at 0.63 and 3.39 μm [52] The bidirectional reflectance distribution function (BRDF) measured scatter in the backward hemisphere.

Polycrystalline materials generally exhibit more bulk scatter than single crystals and glasses. Polycrystalline materials with noncubic crystal structures tend to have the greatest scatter because the refractive index changes from grain to grain (because grains are oriented randomly). This causes a light ray to shift its course as it passes from grain to grain. If the grain size is much smaller ($\leq 1/10$) than the wavelength of light, the scatter by individual grains is not significant. Grain boundaries in polycrystalline materials give rise to scatter because the boundaries generally have a different composition (and different refractive index) from the bulk grain.

6. Mechanical and thermal properties

Table 4 lists mechanical and thermal properties of interest in predicting the performance of optical windows. Unless otherwise indicated, properties apply near 300 K. Although many properties are *intrinsic* to the material, strength, hardness and thermal conductivity are *extrinsic* properties that depend on microstructure and impurities.

The most variable property in Table 4 is strength, which measures the force per unit area required to fracture the material in flexure or tension. A brittle material fractures when the stress exceeds the strength of the weakest flaw that is present, usually at the surface. In general, strength decreases with increasing area under load, because the probability of a

weak flaw being present increases with area. Table 5 illustrates the general observation that strength increases if the surface finish is improved [16,17]. In Table 5, the strength of CaF_2 is more than doubled by improved polishing. The strength also doubles when CaF_2 is annealed, which presumably 'heals' some crystal defects.

In another example of the dependence of strength of surface and bulk treatments, the median strength of sapphire samples increased from 660 MPa to 850 MPa with annealing, to 1120 MPa with noncontact 'superpolishing', and to 1570 MPa with surface ion implantation [79]. The orientation of polishing scratches relative to the tensile axis of a flexure bar also affects strength. Specimens of several different optical materials polished perpendicular to the tensile direction were 20–40% weaker than specimens polished parallel to the tensile direction [80].

Strength can also depend on the atmosphere in which testing is performed, with water and oxygen playing critical roles in the surface chemistry of a developing crack tip as a material fractures. In one example, the strength of ZnS was independent of temperature over the range $-100°C$ to $+600°C$ when tested in dry nitrogen atmosphere [81]. When tested in air, the strength of ZnS increases by 50 [82]–100% [78] when the temperature is raised from 25°C to 500°C.

The strength of a material can depend on its microstructure. Cases are known in which a manufacturer quotes the strength of a material whose microstructure is not optimized for optical performance. A better optical grade of the material might have less strength than that quoted. If strength is critical to a particular design, there is no substitute for measuring the strength of the particular grade of material that will be used with the particular finish that will be used.

Table 5
Effects of surface and bulk treatments on strength of polycrystalline cast CaF_2 [16,17]

Condition	Strength (MPa)	Standard deviation	Number of samples
Set 1: no annealing			
Rough polish (600 grit paper)	42	12	8
Laboratory polish	110	38	15
Optical polish	92	23	15
Set 2: annealed at 900–1000°C in vacuum			
Rough polish (600 grit paper)	88	20	6
Laboratory polish	121	43	15
Optical polish	163	28	12

7. Thermal stress resistance

When a brittle optical window is heated rapidly, part of the window becomes warm and expanded, while other parts are still cool and not expanded. If heating is rapid enough, the stress between the warm and cool regions is sufficient to fracture the window.

Table 6
Thermal shock figure of merit (R') near 300 K[a]

Material	R'
ALON	1.2
AMTIR-1	0.013
Calcium aluminate	0.08
Calcium fluoride	0.17
Fused silica	2.6
Gallium arsenide	7.4
Gallium phosphide	10
Germanium	6.8
MgF$_2$ (polycrystalline)	0.9
Magnesium oxide	2.5[b]
Sapphire	9.7
Silicon	31
Silicon carbide	77
Spinel	1.1
Yttria	1.2
Lanthana-doped yttria	0.6
Multispectral ZnS	2.2
Standard ZnS	2.3
Zinc selenide	1.3

[a] R' is calculated with Eq. (6). An alternative figure of merit that allows stronger materials to be used in thinner structures than weaker materials has been proposed [84].
[b] Using a conservative estimate of strength = 140 MPa.

A figure of merit that describes relative resistance to failure by thermal stress is designated R' [83]:

Thermal stress figure of merit:

$$R' = \frac{\sigma(1 - \nu)k}{\alpha E},\qquad(6)$$

where σ is the strength of the material, ν is Poisson's ratio, k is the thermal conductivity, α is the thermal expansion coefficient, and E is Young's modulus.

Eq. (6) compares the maximum allowable temperature difference ($T_{inside} - T_{outside}$) to which internally heated cylinders made of different materials can be subjected under conditions of convective heat transfer. The maximum allowable temperature difference is proportional to R'. Eq. (6) applies under conditions of 'mild' heating, defined by the condition $bh < k$, where b is the thickness of the material, h is the surface heat transfer coefficient, and k is the thermal conductivity of the material (W/m K). The heat transfer coefficient is the heat entering the material per unit area per unit temperature difference between the atmosphere and the surface (W/m^2 K).

Table 6 gives the thermal shock figure of merit for materials in Table 5 computed with physical properties that apply near 300 K. Since the physical properties generally depend on temperature, and since thermal stress failure generally occurs above 300 K, the R' values in Table 6 should only be considered for their qualitative significance.

Table 6 tells us that the order of thermal stress resistance is SiC > Si > (GaP, sapphire, GaAs and Ge) > (fused silica, MgO, ZnS) > (ZnSe, ALON, Y$_2$O$_3$, spinel, MgF$_2$) > (CaF$_2$, calcium aluminate) > AMTIR-1. SiC offers promise as a thermal-stress-resistant optical window, but it is still developmental and has not yet reached its potential for optical transmission. It is not known whether pure silicon carbide will have a useful midwave infrared transmission window at elevated temperature. Si has very high thermal stress resistance, but its useful upper operating temperature is only 250–300°C because of free carrier absorption. So although Si can be heated rapidly, it cannot be taken to high temperature.

In the next category of materials, GaP has the highest thermal stress figure of merit Its upper use temperature is probably near 600°C, as dictated by free carrier generation. Sapphire is also excellent, but not nearly so resistant as the 300 K value of R' suggests. The strength and thermal conductivity of sapphire fall rapidly above 300 K, so the value of R' for sapphire at a more realistic thermal stress temperature (such as 200–500°C) is much lower than the value in Table 6. Nonetheless, sapphire has the greatest demonstrated thermal stress resistance of commercially available, durable, midwave infrared

Table 7
Observed thermal stress capability of infrared-transmitting domes [85]

Material	Approximate upper limit for stagnation heat flux (W/cm^2)
Sapphire	> 200 (400[a])
Zinc sulfide (standard grade)	> 200 (230[a])
Spinel	> 90 but < 120
ALON	100
Yttria	90
Lanthana-doped yttria	90
Germania glass	45

[a] Theoretical limit for 71-mm diameter hemisphere.

materials [85]. GaAs and Ge also have excellent thermal stress resistance, but their upper operating temperatures are approximately 400°C and 100°C, respectively, due to free carrier generation. GaP and sapphire are therefore the top two candidates for a high-thermal-stress environment.

In the next tier, ZnS is indeed very resistant to thermal stress. Fused silica does not have sufficient bandpass for midwave use and MgO is not a commercially available optical material at this time (although it was formerly produced as hot pressed Irtran-5®). The remainder of the order of thermal stress resistance derived from Table 6 is qualitatively correct. Table 7 gives the observed thermal stress resistance of optical dome materials tested under aerothermal heating conditions in a wind tunnel. Results are consistent with the qualitative predictions of Table 6.

8. Erosion resistance

Optical windows for external use are eroded by high speed impact with rain, and low or high speed impact with solid particles such as blowing sand. Research effort is currently focused on creating durable protective coatings for infrared optical windows.

One way to measure relative rain impact resistance is with a laboratory waterjet. Fig. 13 shows the damage threshold velocity for 300 impacts on the same spot by a waterjet delivered from a 0.8-mm diameter nozzle [86]. The damage threshold velocity for a material is the waterjet velocity below which no damage is observed after 300 impacts and above which damage is observed. ALON is expected to come between spinel and sapphire on this graph. Yttria would probably be near MgF_2. Multispectral ZnS and ZnSe have lower damage threshold velocities than standard ZnS, which is the data point shown in Fig. 13.

Sand erosion is less well understood than rain erosion. As an example of recent work, the behaviors of ZnS and Ge were compared [87]. For perpendicular incidence of 0.3- to 0.6-mm diameter sand at a velocity of 34 m/s, the erosion rate of Ge (expressed as mg of mass lost from the window per kg of sand) was 75% greater than that of ZnS. When the sand velocity was increased to 59 m/s, the erosion rate of Ge was 8% *less* than that of ZnS.

Ge and ZnS are relatively easily eroded. The oxides sapphire, ALON and spinel are much more durable and have generally acceptable rain and sand erosion resistance for subsonic impact speeds. No material has adequate resistance for supersonic rain impacts.

9. Future directions

There remains a need for more thermal-stress-resistant midwave infrared materials. There is also a need for greater erosion and thermal stress resistance in materials that cover both the midwave and long wave regions. The most durable midwave infrared materials (sapphire, ALON and spinel) all have more optical emission than desired at elevated temperature. Chemical-vapor-deposited diamond holds promise for providing thermal stress and erosion resistance in the long wave region, but its midwave absorption and emission rule it out for midwave applications (except as a thin coating). Research in erosion resistance is evaluating both hard and soft coatings. Thermal stress resistance must focus on the bulk window material, because there is no coating that can carry heat away fast enough. SiC, AlN and
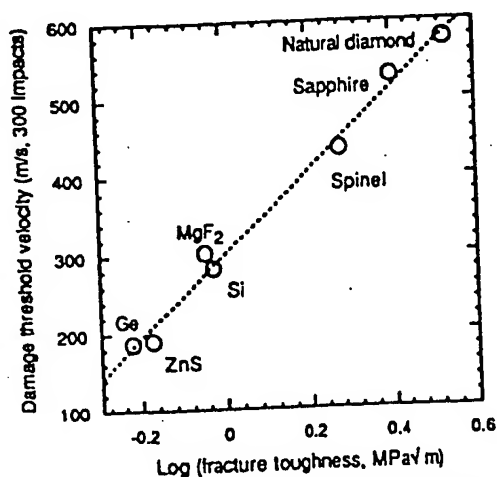

Fig. 13. Waterjet damage threshold velocity (m/s for 300 impacts of a 0.8-mm diameter jet) is correlated with the logarithm of fracture toughness (MPa) of optical materials [86].

Si_3N_4 each promise improved thermal stress resistance (and outstanding erosion resistance), but none is available in a clear, optical form. All three will restrict the available window because of high optical emission at elevated temperature. It is conceivable that the range of material properties could be expanded with nanometer-scale starting materials. In the absence of new materials, improved performance of infrared systems requires engineering innovations to protect the window from the harshest conditions.

Acknowledgements

References

[1] W.L. Wolfe, Optical materials, in: W.D. Rogatto (Ed.), The Infrared and Electro-Optical Systems Handbook, Vol. 3, SPIE Optical Engineering Press, Bellingham, Washington, 1993, pp. 1–78. ISBN 0-8194-1072-1.

[2] W.L. Wolfe, Optical materials, in: W.L. Wolfe, G.J. Zissis (Eds.), The Infrared Handbook, Infrared Information and Analysis Center, Environmental Research Institute of Michigan, Ann Arbor, MI (1985 edn.). ISBN 0-9603590-1-X.

[3] J.A. Savage, Infrared Optical Materials and Their Antireflection Coatings, Adam Hilger, Bristol, 1985. ISBN 0-85274-790-X.

[4] P. Klocek (Ed.), Handbook of Infrared Optical Materials, Marcel Dekker, New York, 1991. ISBN 0-8247-8468-5.

[5] S. Musikant, Optical Materials, Marcel Dekker, New York, 1985. ISBN 0-8247-7309-8.

[6] D.C. Harris, Infrared Window and Dome Materials, SPIE Optical Engineering Press, Bellingham, Washington, 1993. ISBN 0-8194-0998-7.

[7] E.D. Palik (Ed.), Handbook of Optical Constants of Solids, Academic Press, New York, 1985. ISBN 0-12-544420-6.

[8] E.D. Palik (Ed.), Handbook of Optical Constants of Solids, Vol. II, Academic Press, New York, 1991. ISBN 0-12-544422-2.

[9] J.T. Gourley, W.A. Runciman, J. Phys. C 6 (1973) 583.

[10] K.L. Lewis, G.S. Arthur, S.A. Banyard, J. Cryst. Growth 66 (1984) 125.

[11] D.T. Gillespie, A.L. Olsen, L.W. Nichols, Appl. Opt. 4 (1965) 1488.

[12] P. Klocek, T. McKenna, J. Trombetta, Proc. SPIE 2286 (1994) 70.

[13] P. Klocek, J.T. Hoggins, M. Wilson, Proc. SPIE 1760 (1992) 210.

[14] K.V. Ravi, J. Spacecraft Rockets 30 (1993) 791.

[15] F. Schmid, C.P. Khattak, D.M. Felt, Bull. Am. Ceram. Soc. 73 (1994) 39.

[16] R.T. Newberg, J. Pappis, Casting of Halide and Fluoride Alloys for Laser Windows, AFCRL-TR-76-0011. Air Force Cambridge Research Laboratories, Hanscom Air Force Base, MA, February 1976.

[17] P. Miles, Opt. Eng. 15 (1976) 451.

[18] C.A. Klein, R.P. Miller, D.L. Stierwalt, Appl. Opt. 33 (1994) 4304.

[19] S.E. Hatch, Appl. Opt. 1 (1962) 595.

[20] R.M. Sova, M.J. Linevsky, M.E. Thomas, F.F. Mark, Proc. SPIE 1760 (1992) 27.

[21] R.M. Sova, M.J. Linevsky, M.E. Thomas, F.F. Mark, Johns Hopkins APL Technical Digest 13 (1992) 368.

[22] M.E. Thomas, R.I. Joseph, W.J. Tropf, Appl. Opt. 27 (1988) 239.

[23] M.E. Thomas, R.I. Joseph, Proc. SPIE 929 (1988) 87.

[24] M.E. Thomas, R.I. Joseph, Johns Hopkins APL Technical Digest 9 (1988) 328.

[25] M.E. Thomas, Proc. SPIE 1112 (1989) 260.

[26] Optimatr, ARSoftware, 8201 Corporate Drive, Suite 1110, Landover, MD 20785, USA, Phone: 301-459-3773.

[27] A.B. Harker, Emission of Polycrystalline Yttria Between 500 and 1000°C, Rockwell Science Center Report SC5509.FR (Contract N00039-87-C-5301, APL 602698-L), October 1987.

[28] M.J. Dodge, Refractive index, in: M.J. Weber (Ed.), CRC Handbook of Laser Science and Technology, CRC Press, Boca Raton, FL, 1986. ISBN 0-8493-3503-5.

[29] A. Feldman, D. Horowitz, R.M. Waxler, M.J. Dodge, Optical Materials Characterization Final Tech. Rep., Nat. Bur. Standards Spec. Publ. No. 993, 1979.

[30] AMTIR-1 Data Sheet, Amorphous Materials, Garland, TX.

[31] Calcium Aluminate Type WB37A Data Sheet, Sassoon Advanced Materials, Dumbarton, Scotland.

[32] I.H. Malitson, Appl. Opt. 2 (1963) 1103.

[33] H.G. Lipson, Y.F. Tsay, B. Bendow, P.A. Ligor, Appl. Opt. 15 (1976) 2352.

[34] Synthetic Fused Silica Data Sheet, Dynasil, Berlin, NJ.

[35] P. Klocek, M.W. Boucher, J.M. Trombetta, P.A. Trotta, Proc. SPIE 1760 (1992) 74.

[36] W.H. Dumbaugh, Proc. SPIE 297 (1981) 80.

[37] H.W. Icenogle, B.C. Platt, W.L. Wolfe, Appl. Opt. 15 (1976) 2348.

[38] J.C. Richter, C.R. Poznich, D.W. Thomas, Proc. SPIE 1326 (1990) 106.

[39] R.E. Stephens, I.H. Malitson, J. Res. Nat. Bureau Standards 49 (1952) 249.

[40] M.E. Thomas, R.M. Sova, R.I. Joseph, Proc. SPIE 2286 (1994) 522.

[41] C.D. Salzberg, J.J. Villa, J. Opt. Soc. Am. 47 (1957) 244.

[42] D.C. Harris, Development of Yttria and Lanthana-Doped Yttria as Infrared-Transmitting Materials, TP 7140. Naval Weapons Center, China Lake, CA, March 1991.

[43] G.C. Wei, C. Brecher, M.R. Pascucci, E.A. Trickett, W.H. Rhodes, Proc. SPIE 929 (1988) 50.

[44] H.H. Li, J. Phys. Chem. Ref. Data 13 (1984) 103.

[45] N.C. Fernelius, G.A. Graves, W. Knecht, Proc. SPIE 297 (1981) 188.

[46] C.A. Klein, Compendium of Property Data for Raytran Zinc Selenide and Raytran Zinc Sulfide, Report RAY/RD/T-1154, 31 Aug. 1987, Raytheon, Lexington, MA.

[47] D.C. Harris, W.R. Compton, Optical, Thermal and Mechanical Properties of Yttria and Lanthana-Doped Yttria, TP 7002. Naval Weapons Center, China Lake, CA, September 1989.

[48] P.C. Archibald, H.E. Bennett, Opt. Eng. 17 (1978) 647.

[49] D.C. Harris, M.E. Hills, P.C. Archibald, R.W. Schwartz, Rain Erosion Studies of Sapphire, Aluminum Oxynitride, Spinel, Lanthana-Doped Yttria and TAF Glass, TP 7098. Naval Weapons Center, China Lake, CA, July 1990.

[50] D.C. Harris, Comparative Sand and Rain Erosion Studies of Spinel, Aluminum Oxynitride (ALON), Magnesium Fluoride, and Germanate Glass, TP 8147. Naval Air Warfare Center Weapons Division, China Lake, CA, August 1993.

[51] D.D. Duncan, C.H. Lange, D.G. Fischer, Proc. SPIE 1326 (1990) 59.

[52] G.C. Wei, A. Hecker, W.H. Rhodes, Proc. SPIE 1760 (1992) 14.

[53] J.C. Stover, Proc. SPIE 1326 (1990) 321.

[54] E.A. Maguire, J.K. Rawson, R.W. Tustison, Proc. SPIE 2286 (1994) 26.

[55] R. Gentilman, E.A. Maguire, T. Kohane, D.B. Valentine, Proc. SPIE 1112 (1989) 31.

[56] OPTOVAC Handbook 82, OPTOVAC, North Brookfield, MA.

[57] D.N. Batchelder, R.O. Simmons, J. Chem. Phys. 41 (1964) 2324.

[58] Properties of Corning's Glass and Glass Ceramic Families, Corning Glass Works, Corning, NY.

[59] Dynasil Synthetic Fused Silica, Dynasil, Berlin, NJ.

[60] J.S. Blakemore, J. Appl. Phys. 53 (1982) R123.

[61] J.M. Wahl, R. Tustison, J. Mater. Sci. 29 (1994) 5765.

[62] W.H. Dumbaugh, Proc. SPIE 297 (1981) 80.

[63] Germanium Optical Blanks, Union Mineire, Olen, Belgium.

[64] Kodak Irtran Infrared Optical Materials, Eastman Kodak, Rochester, NY, 1981.

[65] M.D. Herr, W.R. Compton, Evaluation of Statistical Fracture Criteria for Magnesium Fluoride Seeker Domes, TP 6226. Naval Weapons Center, China Lake, CA, December 1980.

[66] Optical Properties and Applications of Linde Cz Sapphire, Union Carbide Technical Bulletin, San Diego, CA.

[67] Sapphire, Rotem Industries, Beer-Sheva, Israel.

[68] J.W. Fischer, W.R. Compton, N.A. Jaeger, D.C. Harris, Proc. SPIE 1326 (1990) 11.

[69] D.C. Harris, F. Schmid, J.J. Mecholsky Jr., Y.L. Tsai, Proc. SPIE 2286 (1994) 16.

[70] Y.S. Touloukian et al., Thermophysical Properties of Matter, Vol. 2, IFI/Plenum Press, New York, 1970, p. 97. ISBN 306-67020-8.

[71] D.G. Archer, J. Phys. Chem. Ref. Data 22 (1993) 1441.

[72] Float Zoned Silicon Data Sheet, Amorphous Materials, Garland, TX.

[73] Physical Properties and Critical Constants of Silicon, Silicon Casting, San Jose, CA.

[74] J.S. Goela, M.A. Pickering, R.L. Taylor, B.W. Murray, A. Lompado, Appl. Opt. 30 (1991) 3166.

[75] D.W. Roy, R.G. Martin Jr., Proc. SPIE 1760 (1992) 2.

[76] W.J. Tropf, D.C. Harris, Proc. SPIE 1096 (1989) 9.

[77] CVD Materials, Morton International, Woburn, MA.

[78] F.L.I.R. Grade Zinc Sulfide Data Sheet, Sassoon Advanced Materials, Dumbarton, Scotland.

[79] C.J. McHargue, W.B. Snyder Jr., Proc. SPIE 2018 (1993) 135.

[80] R.W. Rice, J.J. Mecholsky Jr., P.F. Becher, J. Mater. Sci. 16 (1981) 853.

[81] C.S.J. Pickles, J.E. Field, J. Mater. Sci. 29 (1994) 1115.

[82] A.A. Déom, D.L. Balageas, F.G. Laturelle, G.D. Gardette, G.J. Freydefont, Proc. SPIE 1326 (1990) 301.

[83] D.P.H. Hasselman, Ceram. Bull. 49 (1970) 1033.

[84] C.A. Klein, Proc. SPIE 1760 (1992) 338.

[85] J.S. Lin, L.B. Weckesser, Johns Hopkins APL Technical Digest 13 (1992) 379.

[86] C.R. Seward, E.J. Coad, C.S.J. Pickles, J.E. Field, Proc. SPIE 2286 (1994) 285.

[87] J.E. Field, Q. Sun, H. Gao, Proc. SPIE 2286 (1994) 301.

[88] M.E. Thomas, S.K. Anderson, R.M. Sova, R.I. Joseph, Proc. SPIE 3060 (1997) 258.